Power System Simulation Tool for Quick Benchmarking of Innovative MVDC Grids in E-Mobility Applications

Daniel Siemaszko, Philippe Noisette
Hitachi Energy
Spinnereistrasse 3
Turgi, Switzerland
Tel.: +41 79 944 02 99
E-Mail: daniel.siemaszko@hitachienergy.com, philippe.noisette@hitachienergy.com
URL: https://www.hitachienergy.com/

Keywords

« Solid-State Transformer », « Simulation », « Microgrid », « Stability », « Converter control »

Abstract

The rapid development of Solid-State Transformers enables a future for microgrids that features the connection of various sources, loads, and storage elements to a common MVDC bus. The simulation of such systems present various challenges due to their growing complexity caused by the large amount of connected power converters and diversification of sources and loads. Quick benchmarking in booming areas such as E-Mobility typically require simulation models that feature superior speed with a dynamic response that fits real hardware. Within this context and objective in mind, a simulation tool has been developed with system level average models of elementary SST cells for DC grids. The implemented models are built with controlled current/voltage sources which embody dynamic behaviors of real SST systems. They may be arranged in various modular configurations, and they feature a basic failure mechanism that allows bypass of failed cells to study their impact on the full power system.

Introduction

DC microgrids are foreseen to become the backbone of interconnection between decentralized sources, loads and Energy Storage Systems [1]-[3]. It is foreseen that Solid-State Transformers (SST) featuring a DC/DC isolated conversion are to be widely used as elementary building blocks in such DC microgrids. The function of the DC/DC isolated converter can be implemented in at least two well-known ways: a so-called resonant approach with an LLC tank and the isolated Dual Active Bridge (DAB). The choice between the two may be determined based on the application requirements, namely the need for a DC/DC converter with isolation or a DC transformer. The resonant approach has been extensively studied with the introduction of the Power Electronics Transformer (PET) [4]-[8]. Mainly foreseen for traction applications, the resonant approach requires an additional front end for voltage control purposes. The Phase-shift controlled DAB approach has also been well studied and resulted in a 0.5MVA demonstrator [9]. This work showed that the DAB seems better suited for wide voltage applications with its scalability possibilities and easily realized redundancy.

MVDC in E-mobility context

In 2020 the global electric car stock increased by 43% over 2019; about 3 million new e-Cars were registered, electric bus and electric heavy-duty truck (HDT) registrations also increased in China, Europe and North America. Some efforts are underway to develop new standards for mega-chargers (MCS) (i.e Ultra ChaoJi or 3MW chargers), chargers capable of charging trucks or busses reasonably quickly [10]. Some impact to grids is inevitable given the high-power requirements of mega-chargers. Long-term planning for infrastructure is needed now to avoid negative impacts on the electrical grid. Significant investment may be needed for grid reinforcements, renewable integration [11], and energy storage support [12].

On the power system level, the recent development of modular DC structures such as Modular Multilevel Converters (MMC) or Solid-State Transformers (SST) based on Medium Frequency Transformers (MFT), allows to envision a new type of flexible grids that features energy storage and peak sharing, without increasing the available power of substations connected to the grid. The growth of a fleet of electric vehicles in existing facilities requires the installation of energy source such as rooftop solar panels, flexible BESS systems, converters upcoming H_2 fuel cells, and bidirectional chargers for grid support from vehicle batteries.

The foreseen power system would be supported by an MVDC backbone [1], with modular converters interacting the various elements allowing to run on-demand Megawatt Chargers and still rely on renewable energy sources. This is enabled by Battery Energy Storage System (BESS) that act like a buffer for PV, braking energy recovery, and allows limiting power demand from the utility grid. The MVDC grid will also connect local LVDC grids where bidirectional power flow chargers will be operated with la growing number of individual cars [13]-[15].

Considered power system configuration

In this work, a microgrid with ±10kV MVDC backbone (as illustrated on Fig. 1) is presented with the following elements:

- isolated Active Front End (AFE) connecting a 36kVAC utility grid to the ±10kV MVDC link with a so-called Synthetic Inertia that represents the ability of maintaining DC grid stability
- bidirectional SST based converters for connecting the batteries, an LVDC grid used for fast charging of electric cars, and a traction network with breaking energy recovery feature
- unidirectional SST based converters connecting Megawatt Charging loads
- unidirectional SST based converters for supplying PV and H_2 energy to the DC grid
- a so-called Energy Management System that ensures the stability of the bus by engaging the BESS, the fuel cells or the car batteries for grid support.

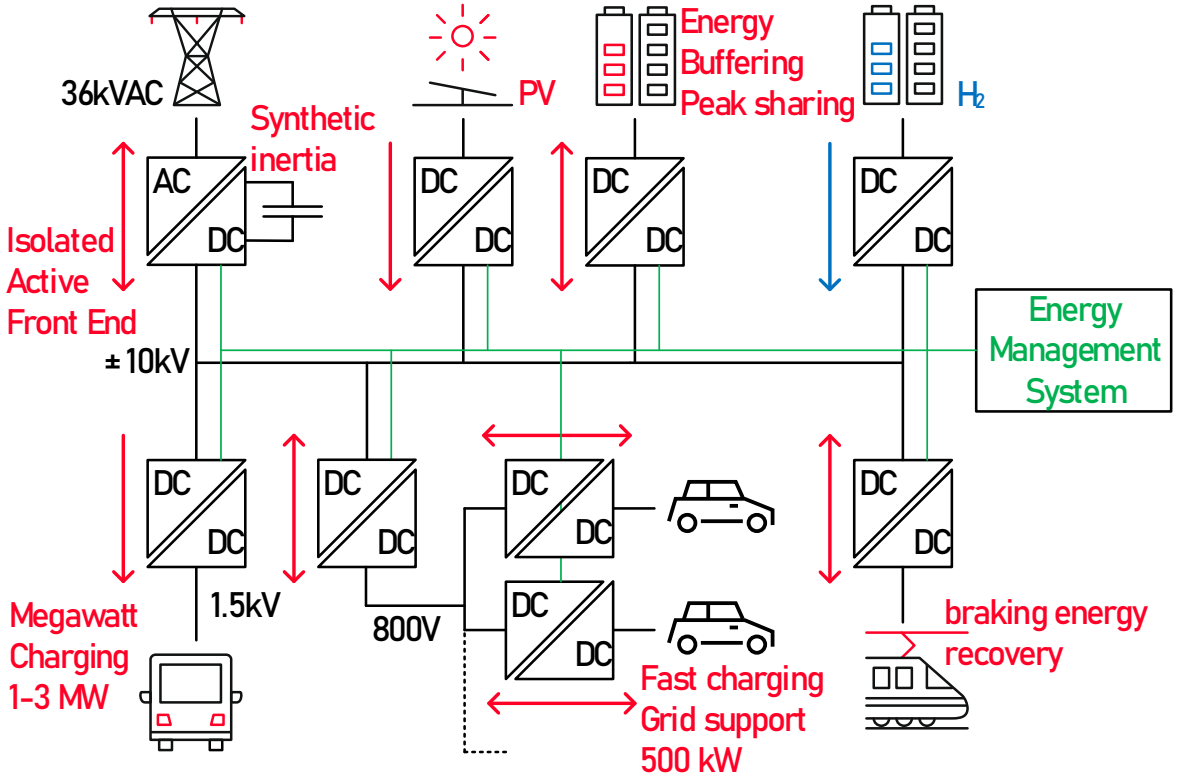

Fig. 1: MVDC network for future E-mobility context

The main elements of the considered system are isolated DC/DC converters that allows modular configurations as illustrated on Fig. 2. The left-hand side figure shows a so-called Input-Series Output-Parallel (ISOP) configuration for reaching high voltages on the one side, and high currents on the fast-charging side. The right-hand side figure shows a simple staked configuration for connecting isolated H_2 fuel cells.

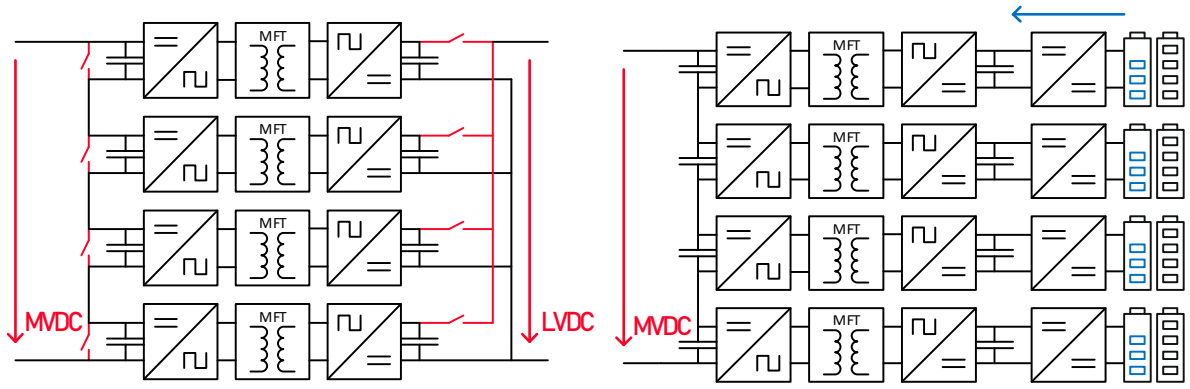

Fig. 2: Typical modular configurations for SST blocks connected

For simulation purpose, the modelling of the system illustrated in Fig. 1 presents a challenge since it is built with a high number of elementary converters, all interacting with each other. On the other hand, a high-level modelling of the system does not consider the dynamic response of the converters. A balance must be found between simulation speed and the level of accuracy one would like to reach. One would like to benchmark several types of configurations, with given scenarios to validate a power system. One would also like to study to impact of a failure of a module on a full system.

Current and voltage source modelling of SST elementary cells

Any power system can be described with their elementary Thevenin-Norton equivalencies, meaning as an arrangement equivalent controlled voltage sources and controlled current sources [16]. Those sources implement an average behaviour of power converters or power sources and can be combined with the condition that some elementary rules are followed. The most important rule is that two voltage sources can't be connected in parallel, and current sources can't be connected in series. A capacitor typically implements the behaviour of a controlled voltage source, and an inductor typically implements the behaviour of a controlled current source. The controls of those sources are typically integrators with multipliers that reflect the behaviour of the modelled elements.

The implemented SST and microgrid models with their current and voltage source equivalents could be run within any power electronics and systems simulation environment. To this specific work, the models have been run with simulation environment Simba.io by Aesim [17]. This environment is a Python based implementation and features a specific Python API which allows building and calling models from Python scripts and programs. This allows all sort of implementation, optimization, pseudo real time operation, and complex post processing with tools that are not available with other simulation environments.

Modelling of the SST elementary Cell

The SST cell is modelled with its equivalent current/voltage source model and can interface power systems that are also modelled as such. Both DC links on each side of the SST are interfaced with controlled voltage sources. The MFT windings are modelled with two controlled current sources. The functions performed by the SST cell are depicted on Fig. 3. As a convention adopted in this work, the SST is connected to a DC grid on its primary side and a current source load on its secondary side.

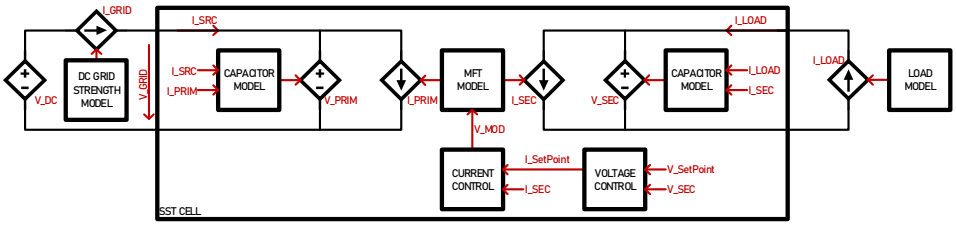

Fig. 3: System level modelling of an SST elementary cell

The dynamics of the system are reflected in the various time constants of the system elements. The behaviour of the capacitors on each side of the SST is modelled as an integrator taking the difference in currents and the capacitance value C_{DC} as described in Equ. 1 and 2. The modulator has a time constant delay defined as a function of switching frequency F_{SW}. The current in the the MFT inductance L_{MFT} is modelled as equivalent transfer function taking the applied voltage V_{MOD} input as in Equ. 3 and 4. The voltage current cascaded PI controllers described by Equ. 5 and 6 are tuned and optimized as a function of the model's physical parameters. The voltage controller maintains the secondary side voltage to a given setpoint, providing a current setpoint. The current controller maintains de MFT current to the given set points by providing the modulation voltage V_{MOD}. The parameters used for running the model are described in Table 1.

$$V_{PRIM} = \frac{1}{C_{DC}} \int (I_{SRC} - I_{PRIM}) \quad (1)$$

$$V_{SEC} = \frac{1}{C_{DC}} \int (I_{LOAD} - I_{SEC}) \quad (2)$$

$$I_{SEC} = \frac{1}{L_{MFT} F_{SW}} V_{MOD} \quad (3)$$

$$I_{PRIM} = I_{SEC} N_{MFT} \quad (4)$$

$$V_{MOD} = K_P (I_{SEC} - I_{SP}) + K_I \int (I_{SEC} - I_{SP}) \quad (5)$$

$$I_{SP} = K_P (V_{SEC} - V_{SP}) + K_I \int (V_{SEC} - V_{SP}) \quad (6)$$

Table I: List of considered SST Cell parameters

	Symbol	Value	Comment
DC nominal voltage on primary side	V_{PRIM}	1000V	Set by grid model V_{GRID}
DC nominal voltage on secondary side	V_{SEC}	2000V	Controlled by SST
nominal current on secondary side	I_{SEC}	250A	Set by load model I_{LOAD}
maximum current on secondary side	I_{SEC_MAX}	300A	Controlled by SST
MFT side SST inductance	L_{MFT}	8.5µH	Defines control's time response
DC side SST capacitor	C_{DC}	3mF	Defines control's time response
MFT switching frequency	F_{SW}	10kHz	Defines control's transfer function

The DC Grid Strength is modelled through its "equivalent impedance" represented by its resistive and inductive components R_{GRID} and L_{GRID} as in Equ. 7. The current source representing the grid impedance interfaces the DC ideal grid voltage source V_{DC} with the primary side of the SST.

$$I_{GRID} = \frac{1}{L_{GRID}} \int (V_{DC} - V_{GRID} - R_{GRID} I_{GRID}) \quad (7)$$

The model is run with a current limiter and anti wind-up on the controller's side. When external load is above SST maximum current specification, typically a burst or a short-circuit, the voltage cannot be maintained on the secondary side. Depending on the direction of the current, a short can be mitigated with or without hitting its own current limiter. On on the left-hand side plot of Fig. 4, the simulation shows the two behavioural cases of an SST running with a short burst on the load side. This allows testing the controller's dynamics in terms of voltage and current control, as well as current limitation capabilities of the model. One can see that the dynamics of the SST cell model correspond to a real SST system when compared with real hardware results from an inhouse built SST demonstrator [9]. Indeed, in both figure the voltage controller time response to a load step is about 7.5ms.

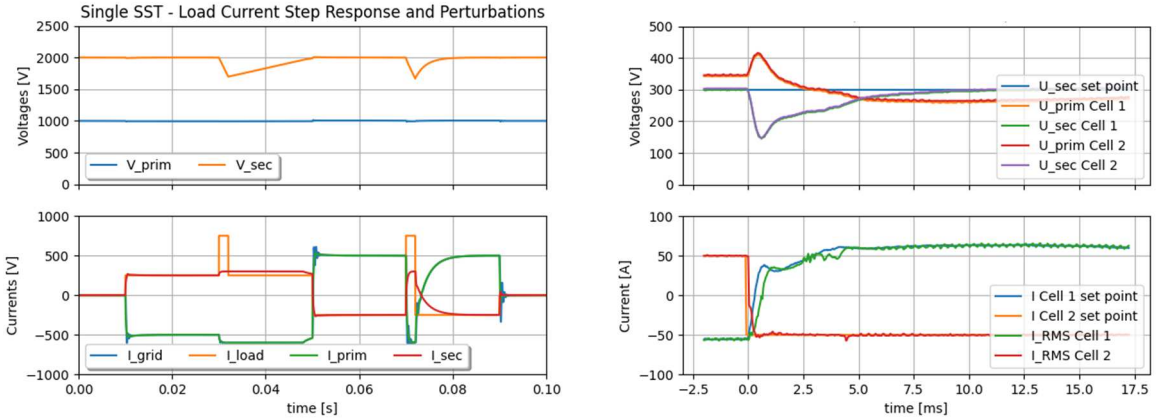

Fig. 4: Voltage and current response of the elementary SST cell with current limiter

Elementary SST connecting a Battery and an Active Front End through a PCC

The same SST Cell as described previously is run with a model of an Active Front End (AFE) on the primary side, and a model of a Battery on the secondary side. As illustrated on Fig 5, a DC bus model is implemented for connecting the two voltage sources, from the AFE and the SST primary side. The DC bus model considers the AFE side as the side providing voltage, and the Passive Front End side (PFE) as the side only drawing current.

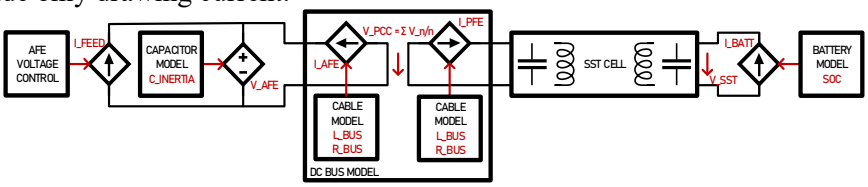

Fig. 5: Modelling of SST cell connecting a Battery to an Active Front End

The Battery is a simple controlled current source; however, it produces current only when its State of Charge (SoC) permits it. SoC should typically vary between 10% and 90% in order to maintain optimal battery lifetime, it is calculated as a function of the integral of the battery current I_{BATT} and the battery capacity Q_{BATT} as given in Equ. 8.

$$SoC = \int \frac{I_{BATT}}{Q_{BATT}} \tag{8}$$

The AFE is modelled as a controlled current source I_{FEED} connected to a controlled voltage source V_{AFE}. Equ. 9 implements the behaviour of a capacitor model C_{AFE} which value represents the inertia of the grid. The AFE current is controlled in a way to maintain the AFE voltage to the voltage set point given by V_{DC} with the use of a PI controller as given in Equ. 10. It features given dynamics, inertia and current limitation set by the system.

$$V_{AFE} = \frac{1}{C_{AFE}} \int (I_{FEED} + I_{AFE}) \tag{9}$$

$$I_{FEED} = K_P(V_{AFE} - V_{DC}) + K_I \int (V_{AFE} - V_{DC}) \tag{10}$$

The DC Bus is connecting voltage sources and must be consequently modelled as current sources. The controls of those current sources implement the dynamic response of a cable with its resistance R_{DCBUS} and line inductance L_{DCBUS}. The model features the voltage of the Point of Common Coupling (PCC), and current sharing between the connected devices. The voltage of the PCC is given by Equ. 11, the currents I_{AFE} and I_{PFE} on both sides of the PCC are given by Equ. 12 and 13.

$$V_{PCC} = \frac{V_{AFE}+V_{PFE}}{2} \tag{11}$$

$$I_{AFE} = \frac{1}{L_{DCBUS}} \int (V_{PCC} - V_{AFE} - R_{DCBUS} I_{AFE}) \tag{12}$$

$$I_{PFE} = \frac{1}{L_{DCBUS}} \int (V_{PCC} - V_{PFE} - R_{DCBUS} I_{PFE}) \tag{13}$$

Fig. 6 shows results of the model run with a load profile reflected by a current set point given to the Battery system. When SoC reaches 90%, the Battery current falls to zero even though the setpoint is set to its nominal value. The AFE is maintaining the DC bus voltage with a "Synthetic Inertia" that is defined by its capacitor model and voltage controller.

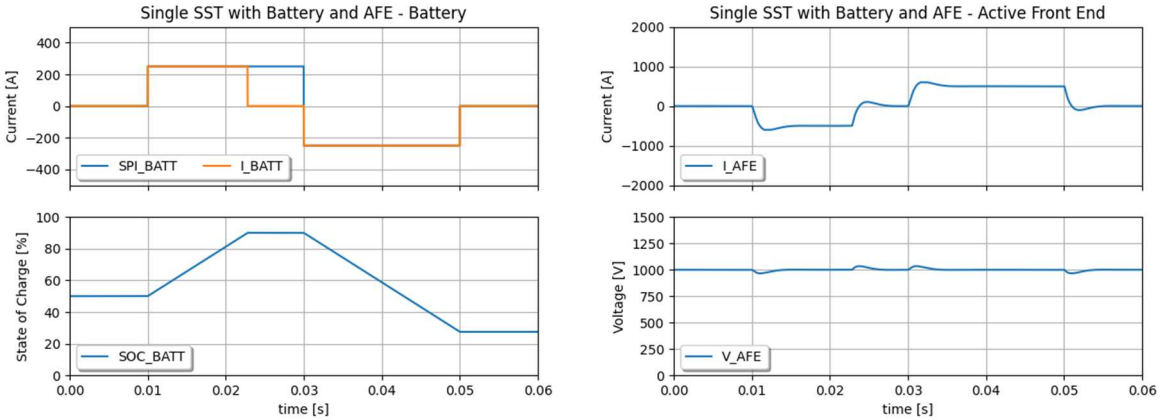

Fig. 6: Voltage and current response of SST cell connecting a Battery to an AFE

Modularity of the SST and Faults

The elementary SST cell described in the previous section can be vertically combined to generate modular configurations, such as Input-Parallel Output-Series (IPOS) and Input-Series Output-Parallel (ISOP) allowing to connect LVDC to MVDC grids [18]-[19]. Each SST cell is working independently and is implemented with bypass capabilities for simulating the effect of a cell fault on the system.

On the MVDC side, the series connection of voltage sources is not a problem. On the LVDC side however, the parallel connection of voltage sources cannot be done without specific attention on the SST local PCC side. Voltage sources must be connected through an arrangement of controlled current sources that reflect the dynamics due to cabling resistance R_{DCBUS} and coupling inductors L_{DCBUS}. This allows generating a PCC voltage that is equivalent to the mean value of all N primary side voltages of all N parallel connected SSTs as in Equ. 14, it also allows current sharing in between the cells, reflecting on what is drawn from the load side, as given in Equ.15. The final current share in between the parallel connected modules is given by Equ. 16.

$$V_{PCC} = \sum \frac{V_{PRIM\_N}}{N} \tag{14}$$

$$I_{GRID} = \sum I_{PRIM\_N} \tag{15}$$

$$I_{SST\_N} = \frac{1}{L_{DCBUS}} \int (V_{PCC} - V_{PRIM\_N} - R_{DCBUS} I_{PRIM\_N}) \tag{16}$$

IPOS configuration with faults

In the 6-cell IPOS configuration illustrated in Fig. 7, the 3-port MVDC side voltage is fully controlled by the sum of individual SST cells. This arrangement allows asymmetric loading on the MVDC side with individual voltage control of both MVDC+ and MVDC- ports. The system is run for demonstration with a fault occurring in one cell to assess voltage and current stability on MVDC side.

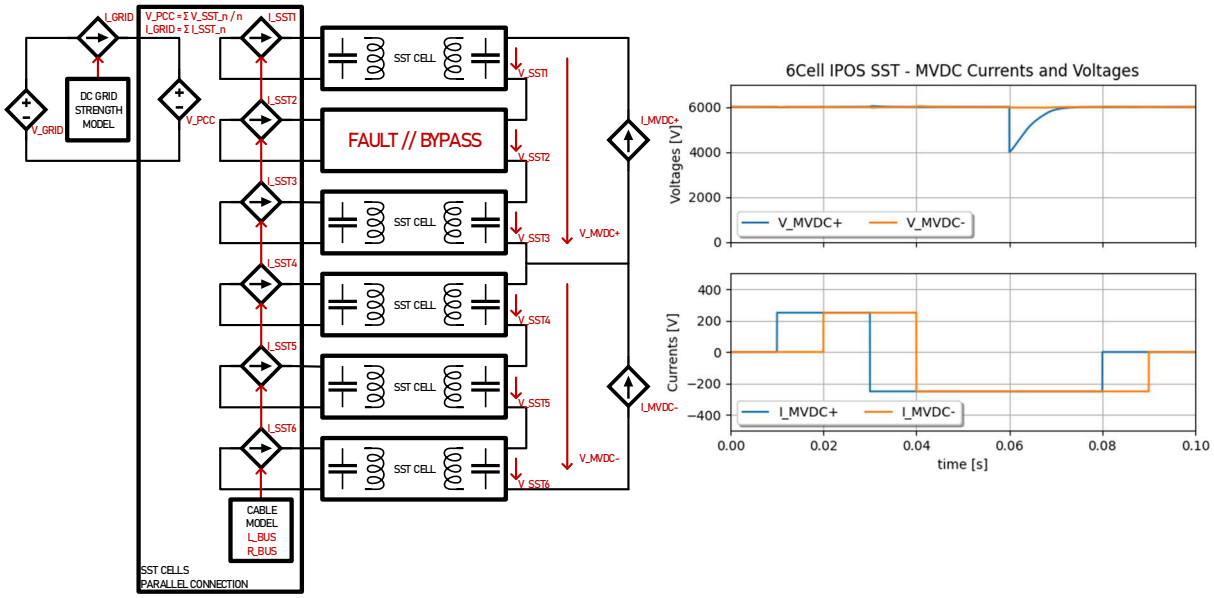

Fig. 7: IPOS configuration of 6 SST cells – Asymmetric loads and fault occurring in one module

Fig. 8 shows currents and voltages on the primary and secondary sides of the SST cells. Asymmetric currents are well distributed among the cells connected to the PCC. At some point, when the two MVDC side currents are opposite to each other, no current is taken from the LVDC grid side as current is only circulating in between the cell via the PCC. When a fault occurs, the MVDC+ voltage is maintained by two cells instead of three, their voltage setpoint is adjusted after the fault occurrence. Theses results show the accuracy of the SST local PCC model for the parallel connection of individual SST cells.

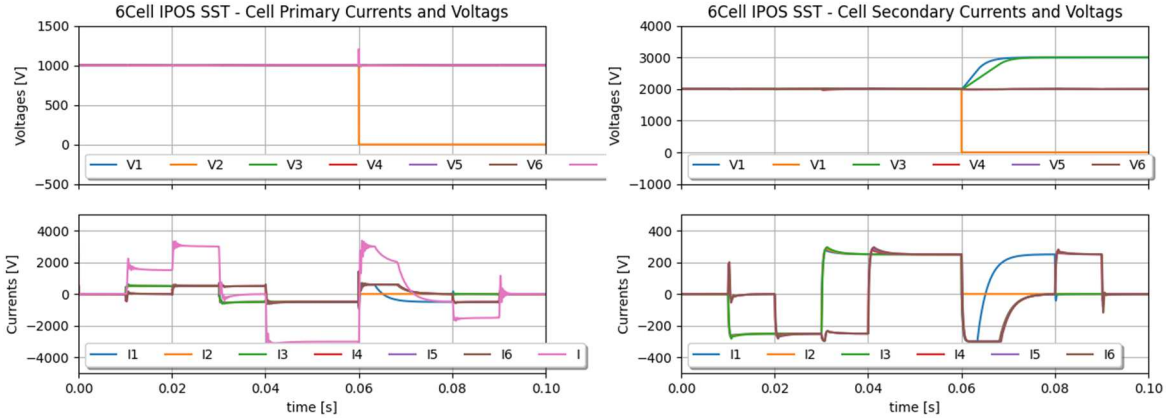

Fig. 8: Current and voltage response of the 6-cell IPOS configuration with a fault

ISOP configuration

The ISOP is slightly different from IPOS in the sense that MVDC side is given by the system and that LVDC side must be controlled. In the arrangement presented by Fig. 9, the LVDC side voltage is controlled by one SST cell, which provides a PCC for the full converter. All other cells control the neutral points voltages on the MVDC side, naturally providing voltage balancing in between the cells.

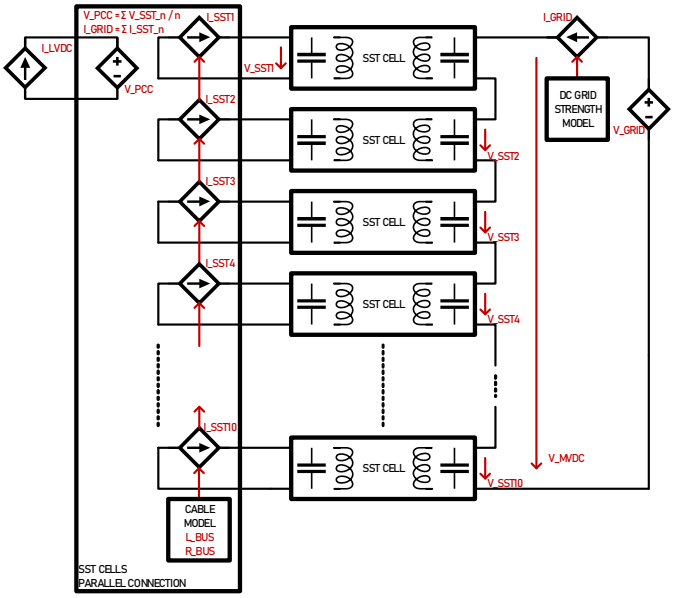

Fig. 9: ISOP configuration of 10 SST CELLs

Results depicted in Fig. 10 show a slight voltage difference between the secondary side voltage of the SST cell that is controlling the LVDC side, because it takes the voltage difference between the MVDC and the sum of all secondary side cell voltages. Otherwise, we foresee excellent voltage and current balancing for this kind of arrangement, as long as one remains within voltage and current limits of the SST cells obviously.

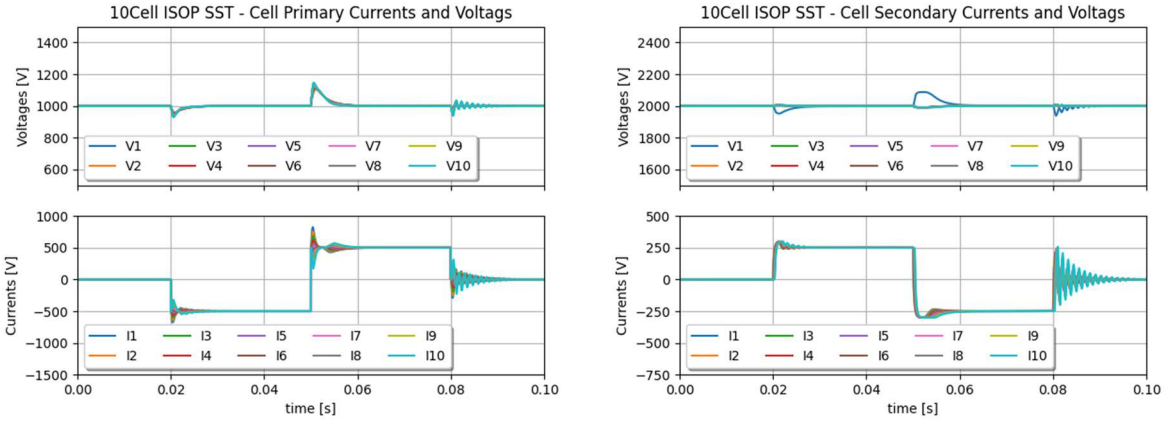

Fig. 10: Current and voltage response of the 10-cell ISOP configuration

MVDC grid model for E-mobility

The power system for the e-Mobility case presented in Fig. 1 is entirely modelled and simulated with the elementary building blocks presented so far. As illustrated on Fig. 11, an MVDC bus interfaces an AFE with several 10-cell ISOP blocks. The AFE maintains the voltage with a dynamic defined by its capacitive inertia and the voltage controller's time constant. One of the 10-cell ISOP blocks interfaces an LVDC bus where single SST blocks are connected for modelling bidirectional fast chargers for car batteries. This model features 73 SSTs working together, it has been implemented with Simba.io the model took less than a minute to simulate 1s simulation time with a time step of 1µs with a quite standard computer.

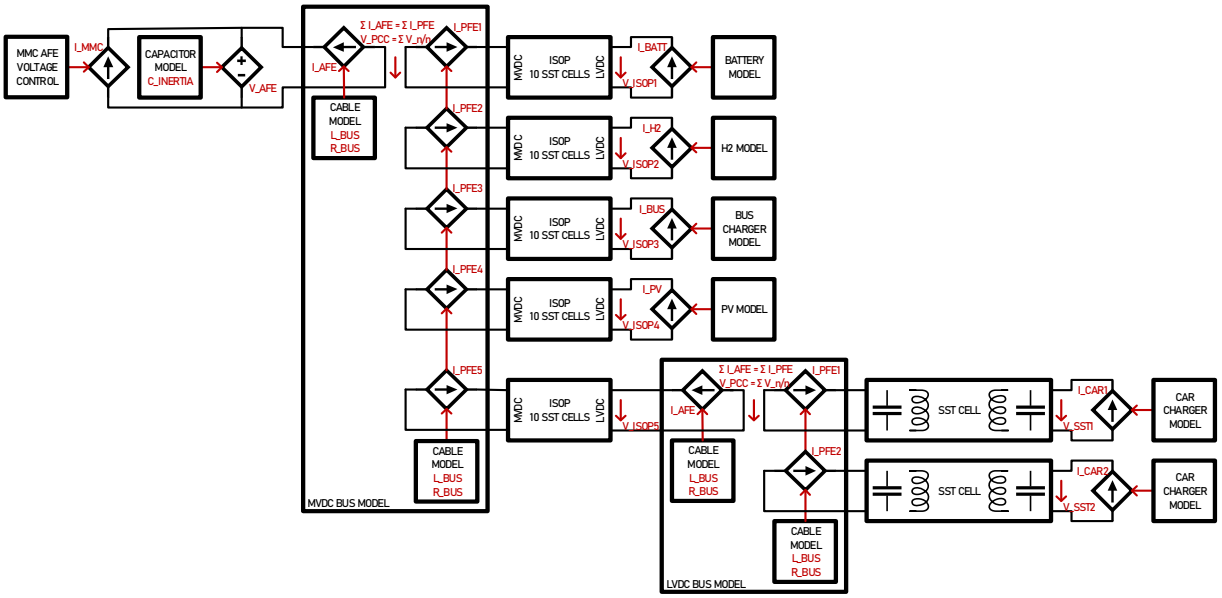

Fig. 11: Modelling of the MVDC grid for E-Mobility context

The simulated scenario involves PV energy drops, grid support from car chargers, and an MMC AFE current limiter for illustrating possible limitations of the system. Fig. 12 shows a run with PVs get covered by clouds, the battery cells fail to work and the AFE can't compensate the full power load. At that point of the scenario, the MVDC bus slightly drops before the car battery kicks in for temporarily supporting the MVDC grid and to save the day.

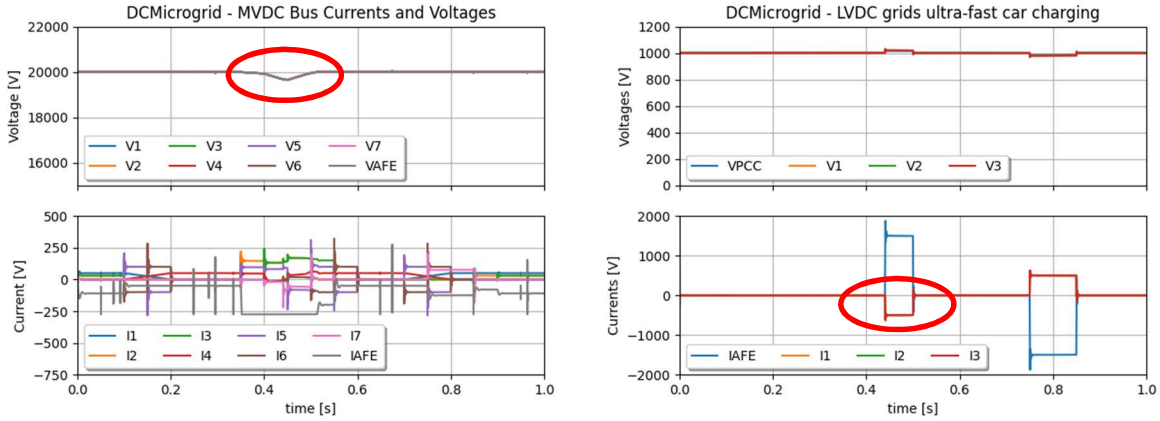

Fig. 12: Current and Voltage response of the MVDC grid for E-Mobility context

Conclusion

This paper presents successful system level modeling of power converter components with their equivalent average models and transfer functions. Their behavior and time response include dynamics of the system and the SST hardware that fits real behaviors. A complex microgrid system with independently controlled elementary SST cells has been simulated. The simulation highlighted some specific DC grid related issues such as DC grid strength and power balancing. The model allows helping the power system design, by evaluating various scenarios and configurations as well as DC protection concept. Also, when evaluating a power system upgrade, one can compare typical CAPEX vs OPEX figures together with functional response of given power systems involving battery storage, H2 fuel cells, and PV cells.

As a prospect, this type of modelling opens up an easy way to quickly simulated various complex configuration in future MVDC power grids, one foreseen application is the booming E-mobility segment that foresees a massive inclusion of renewables and progressive upgrade to DC power.

References

[1] Steinke J. K., Maibach P., Ortiz G., Canales F. and Steimer P.: MVDC Applications and Technology, PCIM Europe 2019; International Exhibition and Conference for Power Electronics, Intelligent Motion, Renewable Energy and Energy Management.

[2] Stieneker M. and De Doncker R. W.: Medium-voltage DC distribution grids in urban areas," 2016 IEEE 7th International Symposium on Power Electronics for Distributed Generation Systems (PEDG).

[3] Mura F. and De Doncker R.W. .: Design aspects of a medium-voltage direct current (MVDC) grid for a university campus, 8th International Conference on Power Electronics - ECCE Asia, 2011.

[4] C. Zhao et al., "Design, implementation and performance of a modular power electronic transformer (PET) for railway application," in Proc. 14th European Conf. on Power Electron. and Applicat. (EPE'11 ECCE Europe), Birmingham, Sep. 2011.

[5] C. Zhao et al., "Power Electronic Traction Transformer—Medium Voltage Prototype," in IEEE Trans. Ind. Electron., vol. 61, no. 7, pp. 3257-3268, July 2014.

[6] C. Zhao et al., "Power electronic transformer (PET) converter: Design of a 1.2MW demonstrator for traction applications," Int. Symposium on Power Electronics Power Electronics, Electrical Drives, Automation and Motion, 2012, pp. 855-860.

[7] D. Dujic, F. Kieferndorf, F. Canales and U. Drofenik, "Power electronic traction transformer technology," in Proc. 7th Int. Power Electronics and Motion Control Conf., 2012, pp. 636-642.

[8] D. Dujic, A. Mester, T. Chaudhuri, A. Coccia, F. Canales and J. K. Steinke, "Laboratory scale prototype of a power electronic transformer for traction applications," in Proc. 14th European Conf. on Power Electron. and Applicat. (EPE'11 ECCE Europe), Birmingham, Sep. 2011.

[9] Heinig S., Siemaszko D., Baumann R. Hubatka N., Klaeusler M., Ruiz R., Burkart R., Yuan C.: Experimental Insights into the MW Range Dual Active Bridge with Silicon Carbide Devices, International Power Electronics Conference IPEC-Himeji 2022 - ECCE ASIA.

[10]Trends and developments in electric vehicle markets, Global EV Outlook 2021, https://www.iea.org/reports/global-ev-outlook-2021/trends-and-developments-in-electric-vehicle-markets

[11] García-Triviño P., Oliveira-Assis L. D., Soares-Ramos E. P. P., Sarrias-Mena R., García-Vázquez C. A. and Fernández-Ramírez L. M.: Configuration and Control of a MVDC Hybrid Charging Station of Electric Vehicles with PV/Battery/Hydrogen System, 2021 IEEE International Conference on Environment and Electrical Engineering and 2021 IEEE Industrial and Commercial Power Systems Europe (EEEIC / I&CPS Europe).

[12] Eldeeb H. H. and Mohammed O. A., Control and Voltage Stability of A Medium Voltage DC Micro-Grid Involving Pulsed Load," 2018 IEEE International Conference on Environment and Electrical Engineering and 2018 IEEE Industrial and Commercial Power Systems Europe (EEEIC / I&CPS Europe.

[13] D. Aggeler, F. Canales, H. Zelaya-De La Parra, A. Coccia, N. Butcher and O. Apeldoorn, "Ultra-fast DC-charge infrastructures for EV-mobility and future smart grids," 2010 IEEE PES Innovative Smart Grid Technologies Conference Europe (ISGT Europe), 2010

[14] M. Dicorato, G. Forte, M. Trovato, C. B. Muñoz and G. Coppola, "An Integrated DC Microgrid Solution for Electric Vehicle Fleet Management," in IEEE Transactions on Industry Applications, vol. 55, no. 6, pp. 7347-7355, Nov.-Dec. 2019

[15] H. B. Sonder, L. Cipcigan and C. E. Ugalde-Loo, "INTEGRATING DC FAST/RAPID CHARGERS IN LOW VOLTAGE DISTRIBUTION NETWORKS," The 12th Mediterranean Conference on Power Generation, Transmission, Distribution and Energy Conversion (MEDPOWER 2020), 2020, pp. 59-65

[16] Barrade P.: Électronique de Puissance, Presses Polytechniques et Universitaires Romandes. 2006

[17] https://simba.io/

[18] J.-W. Kim, J.-S. Yon and B. H. Cho, "Modeling, control, and design of input-series-output-parallel-connected converter for high-speed-train power system," in IEEE Transactions on Industrial Electronics, vol. 48, no. 3, pp. 536-544, June 2001.

[19] L. Heinemann, "An actively cooled high power, high frequency transformer with high insulation capability," APEC. Seventeenth Annual IEEE Applied Power Electronics Conference and Exposition, 2002